FIXED TARGET EXPERIMENTS WITH HEAVY IONS AT CERN*

HELENA BIAŁKOWSKA

Institute for Nuclear Studies
Hoża 69, 00-681 Warsaw, Poland

(Received September 15, 1997)

Recent data on fixed target experiments with relativistic heavy ions at CERN SPS are reviewed.

PACS numbers: 25.75. -q, 12.38. Mh

1. Introduction

Experimental studies of relativistic ion collisions share a distant goal and a broad baseline. The distant goal obviously is Quark Gluon Plasma (QGP), a hypothetical deconfined state of quarks and gluons, predicted by modern lattice QCD. A more modest baseline is a comparison of high energy hadron–hadron, lepton–lepton and lepton–hadron collisions with the collisions of large, bound systems of the above — looking for the origin and physics of the observed differences. With ions large and beam energies high, we hope to create hot, dense and large chunks of matter where partonic degrees of freedom may manifest itself. The fundamental question for an experimentalist is: what would be the signals from such a state — and how to single them out?

My talk will be divided into two parts, the first dealing with leptonic signals from relativistic ion collisions, and the second — with hadronic signals. Throughout the lecture, emphasis will be placed on the experimental findings, with only the necessary amount of theoretical interpretation.

2. Leptonic signals from relativistic ion collisions

In principle, leptons are an ideal probe for nuclear matter. As illustrated in Fig. 1, which depicts various stages of nuclear collision, leptons are pro-

* Presented at the XXXVII Cracow School of Theoretical Physics, Zakopane, Poland, May 30–June 10, 1997.

γ and e^+e^-, $\mu^+\mu^-$ emitted at any time during the collision

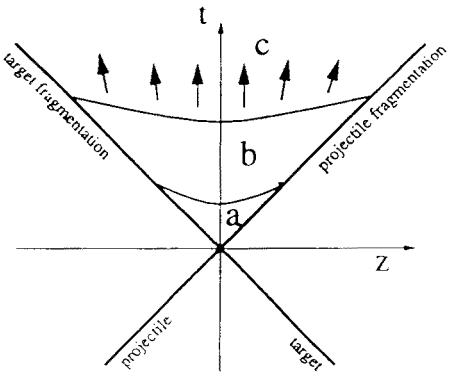

a) formation phase
Drell-Yan mechanism ..

b) hot and dense phase
thermal radiation ..

c) freezeout
hadron decays ..

Fig. 1. Schematic drawing of various stages of nuclear collision

duced during the entire space–time evolution of the system and may bring the information from the early, hot stage. The only problem is how to disentangle this signal from the leptons produced in later stages, by the electromagnetic decays of hadrons.

CERES	e^+e^-	$2.1<y<2.65$	low masses
	p-Be, p-Au, S-Au and Pb-Au data		
HELIOS-3	$\mu^+\mu^-$	$3.5<y$	up to J/Ψ
	p-W and S-W data (completed)		
NA38, NA50, NA51	$\mu^+\mu^-$	$3<y<4$	high masses
	p-A, S-U and Pb-Pb data		

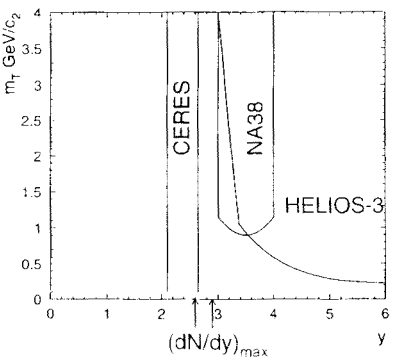

Fig. 2. Dilepton experiments at CERN

In this section I shall review data on direct photon production, electron pair, and muon pair production.

As for direct photons, the situation may be summarized by the statement that in sulphur beam collisions with various targets at 200 GeV/c, within the 90% confidence limit, there is less than 7% room for direct photons [1]. Data from lead beam collisions are still in the analysis stage.

The list of dilepton experiments at CERN [1], together with the respective acceptances in the transverse mass–rapidity variables is presented in Fig. 2. Most of the data come from the midrapidity region, with various cuts in the transverse variable.

2.1. e^+e^- spectra

Since already some time, low mass e^+e^- data are a source of excitement. To start with, let us look at the so called 'cocktail plot' — that is, the mass spectrum of electron pairs from proton-beryllium collisions at 450 GeV/c, as shown in Fig. 3 (note that the invariant mass spectrum is normalized to represent pair density per charged particle density within the rapidity acceptance) [1]. The complicated mass spectrum is reasonably well described by a 'cocktail' of contributions from various electromagnetic decay chan-

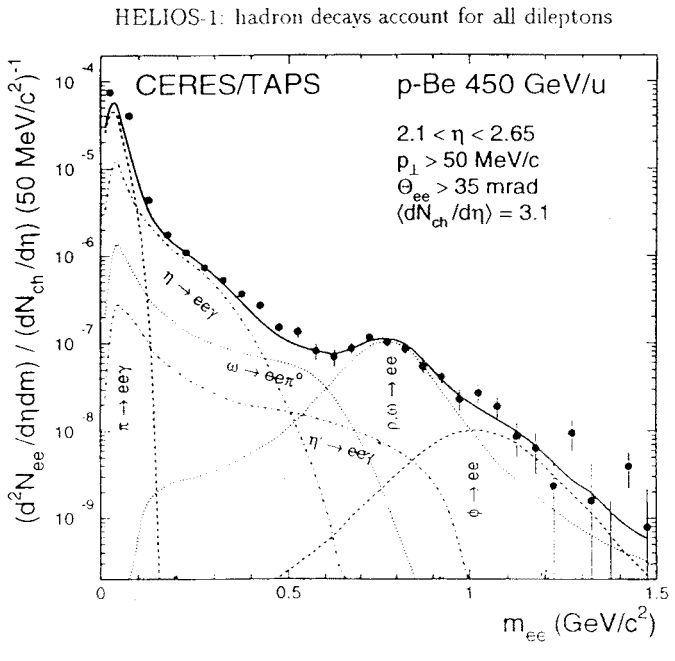

Fig. 3. Dielectrion mass spectrum from p-Be collision

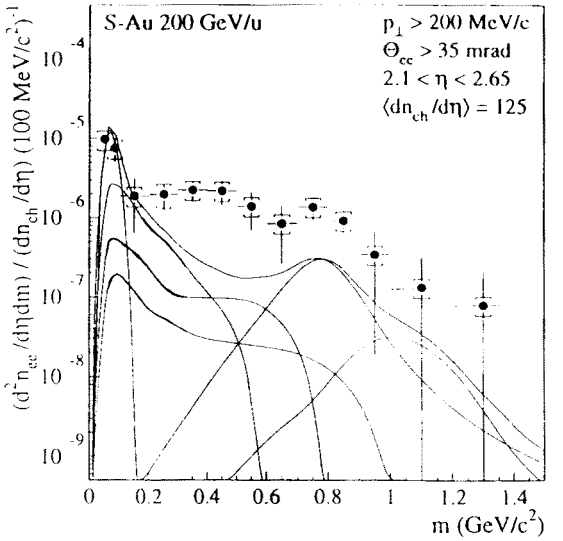

Fig. 4. Dielectron mass spectrum from S-Au collisions

nels, from Dalitz decays of π^0 through ω and η up to ρ, ω and ϕ. Coming now to the same mass spectrum but from nucleus–nucleus collisions, S–Au at 200 GeV/c, shown in Fig. 4, we clearly observe the excess over cocktail contributions in the mass region from 0.2 up to 1.5 GeV. The cocktail contributions known from elementary collisions have been scaled to account for nuclear collisions, using Monte Carlo event generator, with particle ratios of the conventional sources of e^+e^- pairs scaling with the number of produced particles. The enhancement factor over the conventional hadronic contributions is $5.0 \pm 0.7(\mathrm{stat}) \pm 0.2$ (sys).

Fig. 5 shows preliminary mass spectrum of e^+e^- pairs from 160 GeV/c Pb–Au collisions [1]. The solid line shows the sum of cocktail ingredients — contributions from hadron decays, again scaled for nuclear collisions. For masses above 200 MeV the observed spectrum is again significantly higher than the one predicted from hadron decays. The enhancement factor is found to be $2.6 \pm 0.55(\mathrm{stat}) \pm 1.0$ (syst).

Clearly, there are some new phenomena manifesting themselves in the low-to-medium mass range of electron pairs produced in nuclear collisions.

One candidate for such a new phenomenon is thermal radiation emitted from the dense hadronic matter formed in nuclear collisions — $\pi\bar{\pi}$ annihilation into e^+e^- [2,3]. This, however, is not sufficient to describe the observed mass spectrum. Another mechanism would be a long awaited change of resonance parameters in the hot and dense medium — a harbinger of chiral

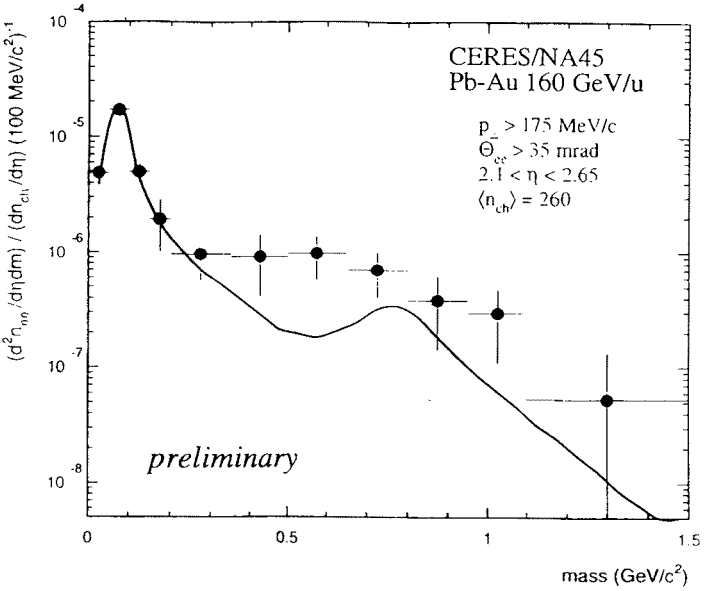

Fig. 5. Dielectron mass spectrum from Pb-Au collisions

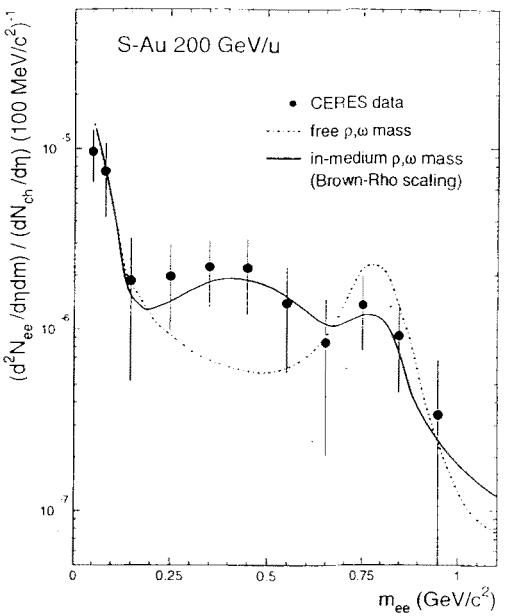

Fig. 6. Influence of the resonance parameters change on the dielectron mass spectra

symmetry restoration. In particular, the ρ and ω mass would be significantly scaled down [4, 5]. Fig. 6 shows that the introduction of such phenomena goes in right direction in describing the observed effect. There is intense theoretical activity concerning the details of the proposed mechanisms.

2.2. $\mu^+\mu^-$ spectra

Here I shall concentrate on the hot subject of heavy quarkonia production and suppression in high energy nuclear collisions, leaving aside an important subject of thermal dimuons and observed excesses (over conventional expectations) in dimuon mass spectra in the intermediate mass region.

A word on history might be in order. A decade ago Satz and Matsui [6] called attention to the possibility of direct observation of a clear QGP signal if a strong suppression of J/ψ production in central nuclear collisions could be detected. Such effect indeed was observed in 1986 in O–U and in 1987 in S–U collisions, [7] stirring much excitement. Soon, however, classical explanations were proposed, without quark gluon plasma.

Since that time much progress has been made, both in experiment and theory.

On the experimental front, Fermilab measurements of absolute cross sections of direct J/ψ and ψ' production in hadronic collisions [8] appeared by

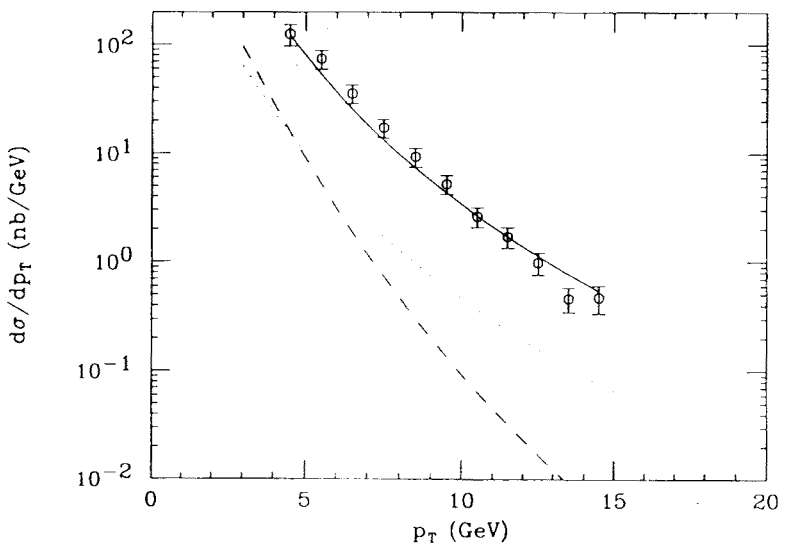

Fig. 7. Fermilab CDF data on differential cross section for prompt ψ production. Dashed and dotted lines are colour singlet contributions, solid line gives the colour octet mechanism contribution.

an order of magnitude too high compared with the so-called color singlet model.

It thus appeared that in the so-called operator product expansion technique, used to describe the $c\bar{c}$ pair production, an important contribution comes from a color octet term (a color octet $c\bar{c}$ plus a gluon) [9]. Fig. 7 shows the Fermilab data on direct J/ψ production, together with color singlet and color octet descriptions. This clearly demonstrates the need for a new, octet term.

The color octet scheme bears profoundly on the J/ψ (and ψ') production in nuclear collisions, as it translates directly into nuclear absorption cross sections. If $c\bar{c}$ hadronization occurs in an extended strongly interacting medium, the 'pre-resonance' state does not know whether it will turn out as J/ψ or ψ' outside the medium. Kharzeev and Satz [10] have calculated the effective absorption cross section of such pre-resonances in matter to be 6 mb, and have succesfully described both J/ψ and ψ' attenuation in p–nucleus collisions, as shown in Fig. 8. In this figure a compilation of relative J/ψ, ψ' and Υ attenuation on nuclear targets is shown as a function of the L variable, suggested by Gerschel and Hufner [11]. L is calculated as an average length of the path of the particle in nuclear matter, and thus parametrizes various nuclear targets.

Coming now to nucleus–nucleus collisions [12], we see in Fig. 9 the experimental data on J/ψ production relative to the Drell–Yan yield, shown together for proton, sulphur and lead collisions on nuclear targets, again as a function of L. All data points fall onto the 6 mb absorption line — with notable, and some say, extraordinary exception of lead on lead points. Consecutive data points for Pb on Pb were determined for various degrees of centrality of collisions, as measured by the associated transverse energy. Different presentation of the same data is shown in Fig. 10, [13] where instead

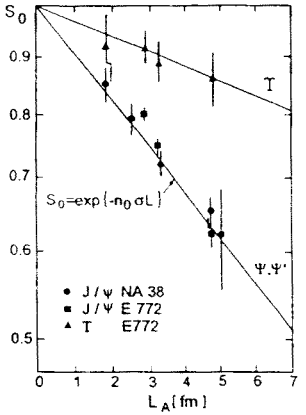

Fig. 8. Quarkonia suppression on nuclear targets

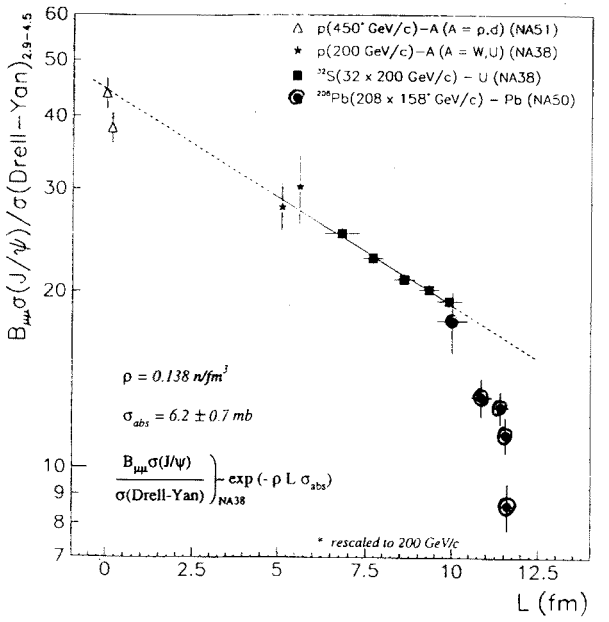

Fig. 9. ψ production cross section relative to the Drell–Yan yield in nuclear collisions as a function of the path length of $c\bar{c}$ pair in nuclear matter.

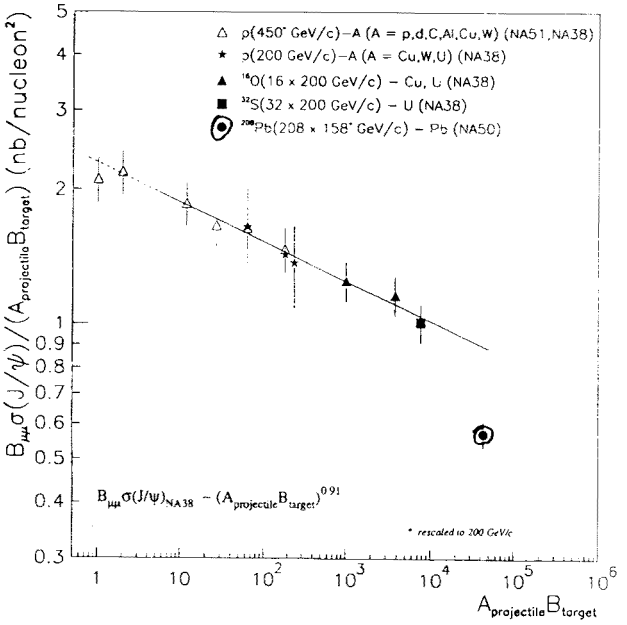

Fig. 10. ψ production cross section in nuclear collisions as a function of projectile and target mass number.

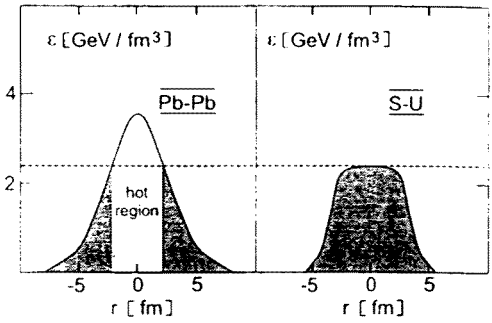

Fig. 11. Radial density profiles for central Pb-Pb and S-U collisions

of the model dependent L variable, the product of atomic mass numbers of the colliding objects is used as an abscissa.

Apparently, in lead on lead collisions at 158 GeV/c an additional J/ψ suppression mechanism is at play. The average energy density, as evaluated for S–U and Pb–Pb collisions does not differ significantly. However, as suggested by Blaizot and Olitraut [15], the differential radial density profiles differ in both cases. As sketched in Fig. 11, there is a flat density profile for S–U, whereas for Pb–Pb the distribution is peaked, thus allowing for higher values of energy density for the most central collisions. This central hot region may suffice to create a new partonic state, where Debye screening prevents the creation of bound J/ψ resonance. According to Kharzeev [14], The NA50 Pb–Pb results indeed seem to suggest that a new mechanism of J/ψ suppression sets in at higher energy densities. The observed effect can be considered as a strong indication for some kind of deconfinement in nuclear collisions. The question 'what can we do to turn this indication into a proof, or to discard it?' sets a line for future experiments (and theoretical developments as well).

3. Hadronic signals from relativistic ion collisions

In this section I shall cover the following topics:
1. Longitudinal hadronic spectra and the stopping power.
2. Transverse hadronic spectra and their relation to temperature and flow.
3. Strange particle production.
4. Source sizes as determined by interferometry.

3.1. Stopping

Stopping is essentially an intuitive term, introduced in order to describe to what extent two large colliding objects — nuclei — stop each other, or

remain transparent, and 'go through'. Various methods of stopping evaluation have been proposed and used. A poor man's stopping determination is performed by a calorimetric measurement of the transverse energy of particles emitted in the collision. Were there a full stopping, an isotropic energy distribution should be observed, with no preference given to the initial beam direction. In this case the maximum value of the transverse energy $E_{T\max}$ should equal

$$\frac{\pi}{4}\sqrt{s} - m(\text{participants}) .$$

The transverse (hadronic) energy is usually measured in some limited rapidity range, and has to be extrapolated to the full phase space region. An illustration of the transverse energy distribution, measured in S–Au and Pb–Pb collision in the CERN experiment NA49 [36], is shown in Fig. 12.

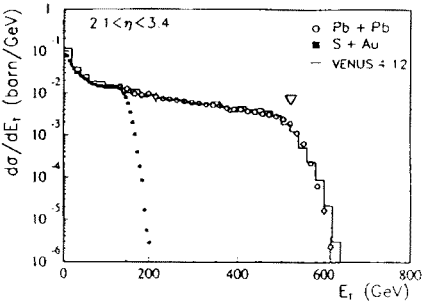

Fig. 12. Transverse energy spectrum from Pb-Pb and S-Au collisions

After extrapolation to the 4π and evaluation of the number of nucleon participants, one can determine relative stopping as $S_r = E_T/E_{T\max}$. The NA49 measurements give the following estimate:

Nuclei	S_r
S S	0.47
S Au	0.52
Pb Pb	0.57

all with an error about 10%. Thus roughly half of the incident energy is 'stopped' in the collision.

In a more differential approach one may ask: do the participating baryons stop?

In order to answer, one has to measure the rapidity distribution of baryons minus antibaryons, or , specifically, protons minus antiprotons.

Experimentally, the procedure to determine the net baryon rapidity distribution, is a multistep process. It is perhaps a good place to make a

comment on essentially two types of experiments to study the products of heavy ion collisions. In one type, exemplified by the NA49, the detectors cover as much as possible of the entire 4π phase space, registering practically all hadrons produced (together with their weak decay products), and determining their momenta. This is no mean feat, taking into account that the charged particle multiplicity in lead on lead collisions at 158 GeV/c goes into thousands (about 2500 in central collisions). Particle identification for individual reaction products is rarely possible, but in selected areas of the phase space it is performed on the statistical basis, using additional quantities such as dE/dx measurements and combining them with time-of-flight information.

Another type of experiment, exemplified by NA44, limits the detection of particles to a rather limited sector of the entire phase space, but makes up for that with very sophisticated particle identification equipment, allowing for good separation of most of the hadrons produced.

There is another experimental aspect of relativistic ion experiments, which needs clarification. Data are often shown as 'central', 'semi central' *etc.* Obviously one would like to select the reactions with minimum impact parameter, or head-on collisions, but there are only indirect methods of the centrality determination. Usually experiments are triggered either on the transverse energy produced (the larger it is, the more central the collision) or the absence of the forward energy deposit. The only honest way to quantify the centrality is to give the percentage of the total inelastic cross section accepted by a given centrality trigger. This can be translated into a given range of impact parameters only in a model dependent way — usually just calculating it in the geometrical picture of A (incident nucleus) nucleons incident on B (target nucleus) nucleons.

Coming back to the net proton rapidity spectra, an example is shown in Fig. 13, coming from NA49 [16]. In order to produce this result, several steps were taken. First, the positive and negative particle spectra have been measured (in one half of the CM system, but then the system is reflection symmetric). Then, with appropriate rapidity calculation, negative particle spectrum was subtracted from the positive particle spectrum (this tacitly assumes an identical shape of positive and negative pion spectra, and as a first approximation, neglects other charged hadrons). To this subtracted spectrum corrections were applied in order to account for charged kaons, and for protons coming from lambda hyperon decays. And, of course, detector acceptance was taken into account.

A comparison of the net proton rapidity spectrum from Pb–Pb collisions, shown in Fig. 13, with the similarly determined net proton spectrum from S–S collisions (scaled by the ratio of the number of participants in the two cases), reveals a significant change in going from light to heavy colliding

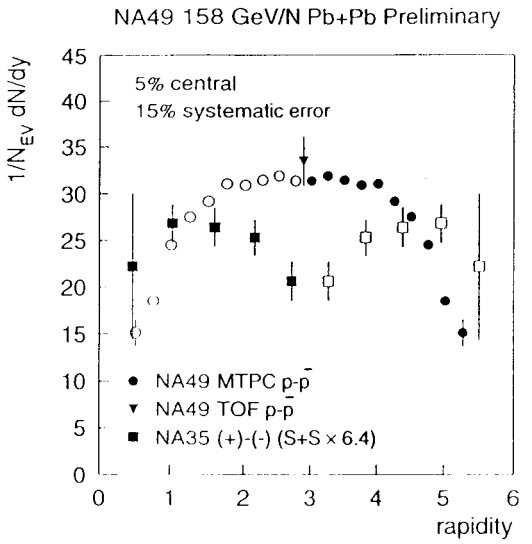

Fig. 13. Net proton rapidity spectrum from central nuclear collisions

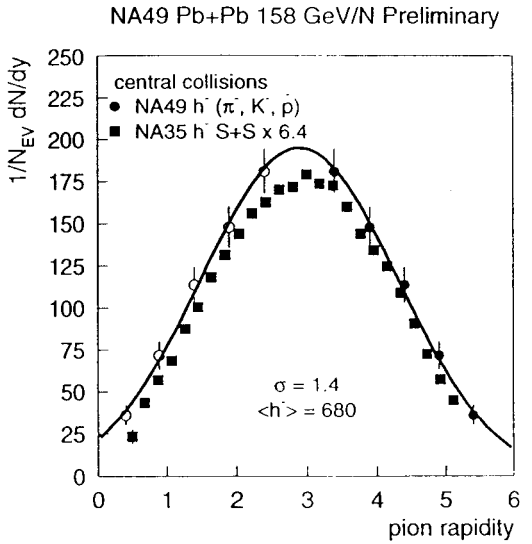

Fig. 14. Negative hadron rapidity spectrum from central nuclear collisions

objects. A rapidity plateau is seen for lead on lead collisions, implying more stopping of baryons.

The rapidity spectrum of negative hadrons (90% of which are pions), shown in Fig. 14, displays a gaussian-type shape, similar for S-S and Pb-Pb central collisions. These spectra are still wider than what one would expect for an isotropic fireball, indicating an elongation of the source along the beam direction.

3.2. Transverse spectra

The transverse particle spectra, measured for various particle species, offer up a rich material for interpretation. The bare facts are such that (with the exception of low p_T pions) all transverse spectra are to a good approximation, exponential, and the inverse slope parameters, carelessly sometimes called 'temperature', do depend on the particle mass/type. This is illustrated in Fig. 15 and Fig. 16 [17,21]. This mass dependence is often interpreted as a reflection of the collective transverse flow from expansion of the system produced. In the hydrodynamical picture matter flows and particles of different masses move with the same velocity. The experimental slope parameter measures both thermal and collective contributions. The intrinsic freezeout temperature is determined by the thermal motion. The NA44 experiment has fitted their data on the slope parameters for S–S and Pb–Pb with a very simple two parameter function, assuming linear dependence of the slope on the average squared transverse velocity. The freezeout temperature of approximately 140 MeV and average transverse expansion velocity of 0.2–0.3 for S–S and 0.4 for Pb–Pb have been obtained (Fig. 16).

A forthcoming NA49 publication [18] combines the information from the Bose–Einstein correlations with that of the transverse mass spectra of hadrons produced in central lead on lead collisions, and finds a consistent picture for the evolution of the particle emitting source with transverse radial velocity field characterized by $\beta_T = 0.6$–0.7.

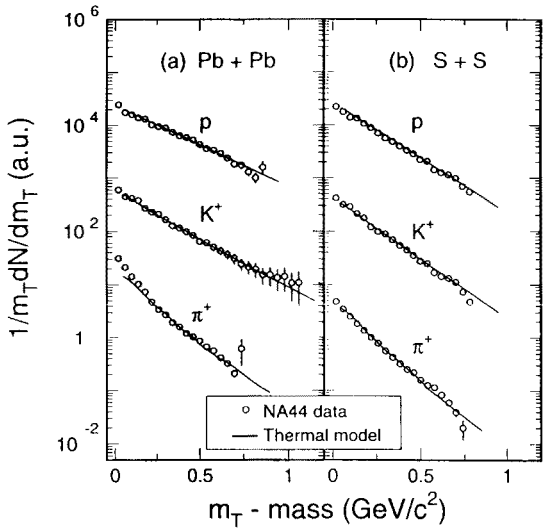

Fig. 15. Transverse mass distributions for pions, kaons and protons from nuclear collisions.

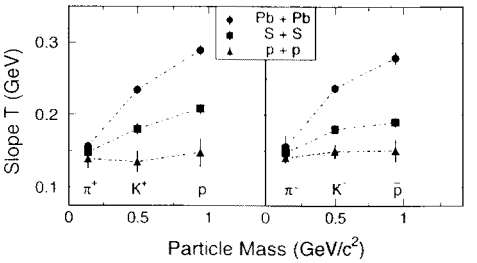

Fig. 16. Slope parameters of the transverse mass spectra as a function of particle mass.

The hydrodynamic interpretation is by no means a unique one. Alternatively, Leonidov, Nardi and Satz [19] show that mass dependence of transverse slopes can result from broadening of transverse distributions by 'random walk initial state collisions' — a superposition of longitudinal, boost invariant, isotropically decaying fireballs. The transverse fireball motion is determined by hadron–nucleus data and extrapolated to nucleus–nucleus collisions.

3.3. Strangeness production

In standard leptonic/hadronic collisions, the ratio of $u\bar{u}$ to $d\bar{d}$ to $s\bar{s}$ pair production is given by

$$u\bar{u} : d\bar{d} : s\bar{s} = 1 : 1 : \lambda$$

with λ, the strange quark suppression factor, approximately independent on colliding objects, slightly increasing with s, and equal 0.2–0.3 for $\sqrt{s}$ greater than 10 GeV.

It has long been expected that if the Quark Gluon Plasma is produced, the high parton density and lower energy threshold for $s\bar{s}$ production would increase λ. Data from light ion collisions (central S–S at 200 GeV/c) have indeed shown an increase in strange particle production, as compared to hadron-hadron and hadron-nucleus collisions. The effect can be seen in Fig. 17 [20], where the strangeness suppression factor has been determined on the basis of full strange and non-strange particle multiplicities for different sets of colliding objects at 200 GeV/c. The procedure involved in the λ determination required the extrapolation of multiplicity data to the 4π acceptance.

Preliminary data from Pb–Pb collisions at 158 GeV/c give information on the open (K, Λ and Ξ) and hidden (ϕ) strangeness production in limited areas of the phase space. Within the still large (20%) errors, the strangeness enhancement seen for S–S, persists in central Pb–Pb collisions, but does not increase [21].

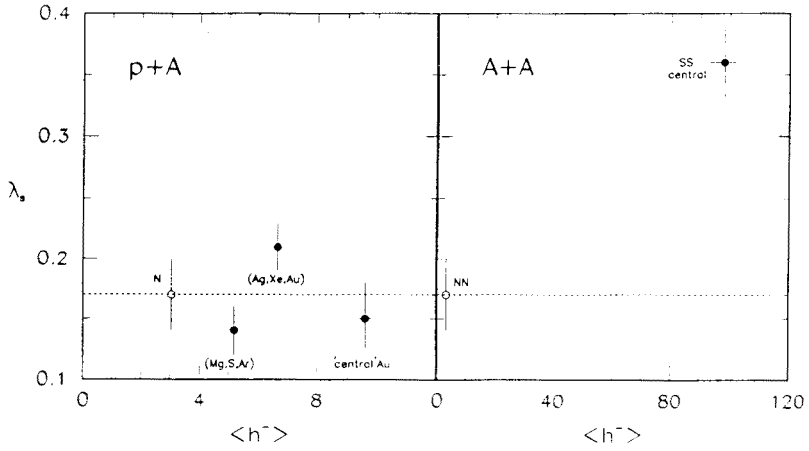

Fig. 17. Strange quark suppression factor for hadron-nucleus and nucleus-nucleus collisions.

The following figures, taken from NA49 [21], show various aspects of the strangeness production. Fig. 18 shows the ratio of kaons to pions, evaluated for various sets of colliding objects, as a function of the estimated number of participants in the collision.

Fig. 19 shows first information on the lambda hyperon rapidity distribution in Pb–Pb collisions, and Fig. 20 that on the antilambda. For comparison, lambda/antilambda rapidity distributions are shown for S on S collisions and for proton-proton. The antilambda distribution does not change much between the collisions of light to heavy systems, but for lambdas the change is dramatic. Instead of two peak structure in S-S we find a broad maximum centered at midrapidity in Pb-Pb. This falls in line with the observed change in net proton spectra, and is consistent with formation of a baryon rich region at midrapidity.

Preliminary values of various particle production ratios have been determined, important for thermodynamical description of reaction mechanism. Data from NA49 Pb–Pb give K^+/K^- about 1.8 and $\Lambda/\bar{\Lambda}$ about 0.2 [21].

There are also first data on the ϕ production. The ϕ is almost a pure $s\bar{s}$ state and serves as a good source of information on strangeness production. In S-U collisions a significant increase of ϕ production compared with other vector mesons, ρ and ω, has been observed [22]. There is also an interest in the values of ϕ mass, width and branching ratios for various decay modes as observed in nuclear collisions, because of predictions of possible changes in these parameters influenced by nuclear medium [24].

The ϕ meson has been observed in the NA49 experiment in Pb-Pb collisions [23] through its hadronic decay into K^+K^- (49.1%). At midrapidity a relatively clear kaon identification is obtained by combining the dE/dx in-

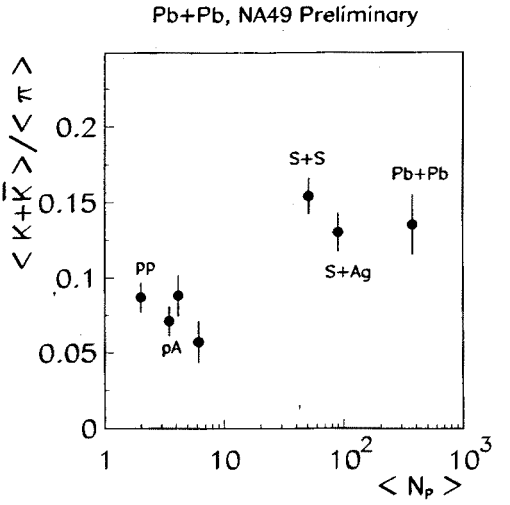

Fig. 18. Kaon to pion ratio from nuclear collisions as a function of the number of participant protons.

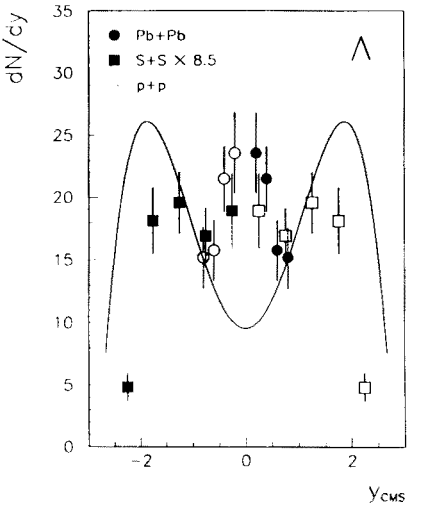

Fig. 19. Λ rapidity spectrum from nuclear collisions

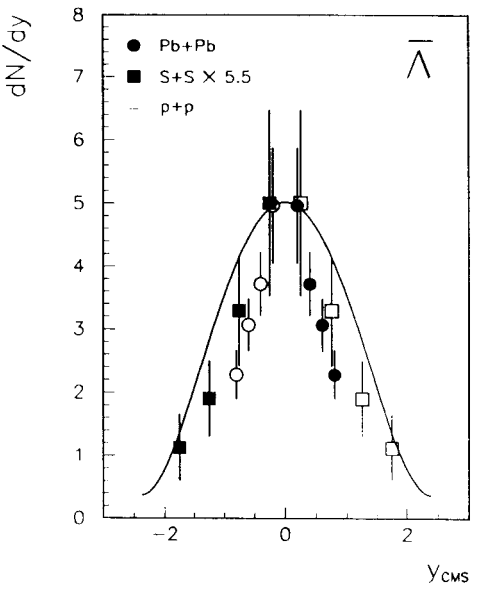

Fig. 20. $\bar{\Lambda}$ rapidity spectrum from nuclear collisions

formation with the time of flight (TOF). In the forward rapidity region the dE/dx information helps to reduce the pion background. Fig. 21 shows the K^+K^- invariant mass spectrum from dE/dx separated kaons, after background subtraction. There is as yet no indication of a resonance parameter change. As for the evaluation of the total ϕ yield, there is no indication of an enhancement, but the errors are large, and one awaits a significant increase in the statistics, to be analyzed soon.

A very important source of information on the state formed in high energy nuclear collisions is the production of cascade hyperons, or multi-strange particles. It has been suggested [25] as a useful probe of the early phases of the collision, since 'normal' hadronic production of such particles is strongly suppressed due to high mass thresholds.

Most of the CERN data on cascade production come from a series of experiments WA85, WA94, WA97, dedicated to the study of strangeness. Neutral strange particles are identified by their charged decay products in a magnetic field. The geometrical acceptance is the same for particles and antiparticles and covers the region of central rapidity and medium transverse momenta.

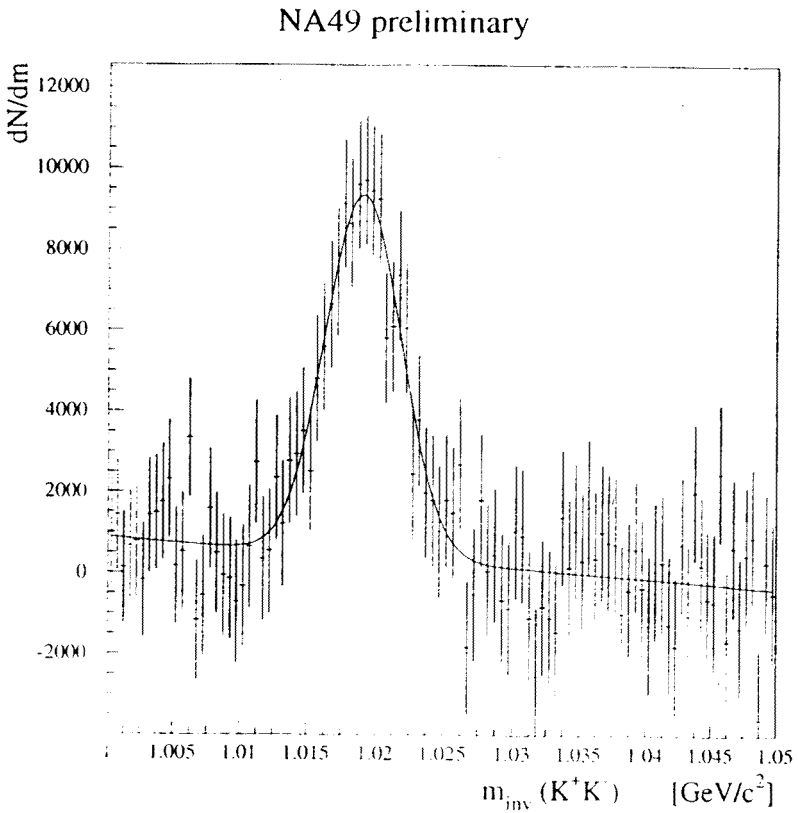

Fig. 21. K^+K^- mass spectrum from dE/dx identified kaons, background subtracted. The solid line is a Gaussian fit with mass of 1019.1± 0.3 MeV/c^2.

Fig. 22 shows a compilation of cascade to lambda hyperon (and the corresponding antiparticle) production ratio in proton–proton, proton–nucleus and nucleus–nucleus collisions. A clear increase of these ratios is observed in nuclear collisions [26]. An increase of an enhancement of strange particles in nuclear collisions with respect to proton–nucleus collisions (normalized to the yield of negative particles) is more pronounced for multi-strange particles, as seen in Fig. 23. Very preliminary data on the cascade production in Pb–Pb collisions [27] give the first hint of an even more pronounced effect in the Ω production rate. Fig. 24 shows the Ξ and Ω signals in p-Pb and Pb-Pb collisions, as measured by WA97. The ratio of Ω/Ξ increases by a factor of about 3 when going from p–Pb to Pb–Pb.

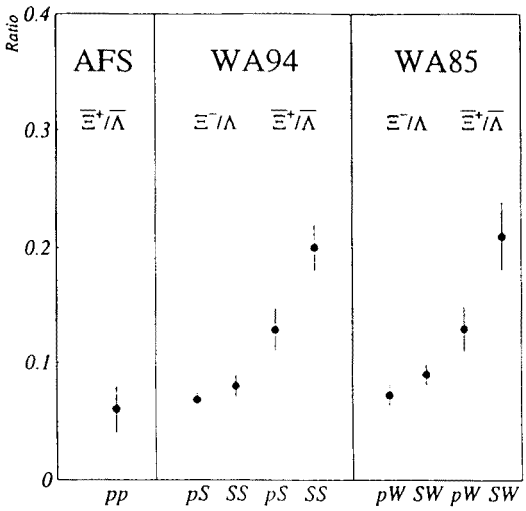

Fig. 22. Cascade to lambda hyperon production ratio from nuclear collisions

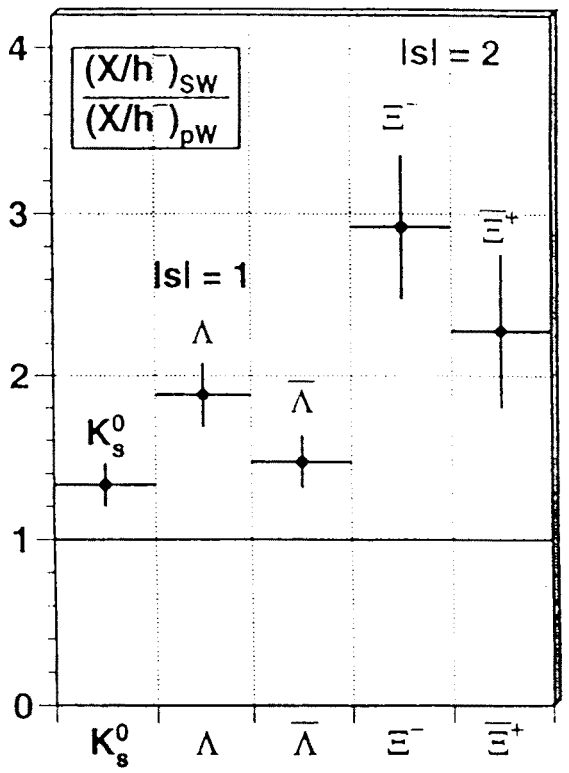

Fig. 23. Enhancement of strange particles in S-W with respect to p-W collisions

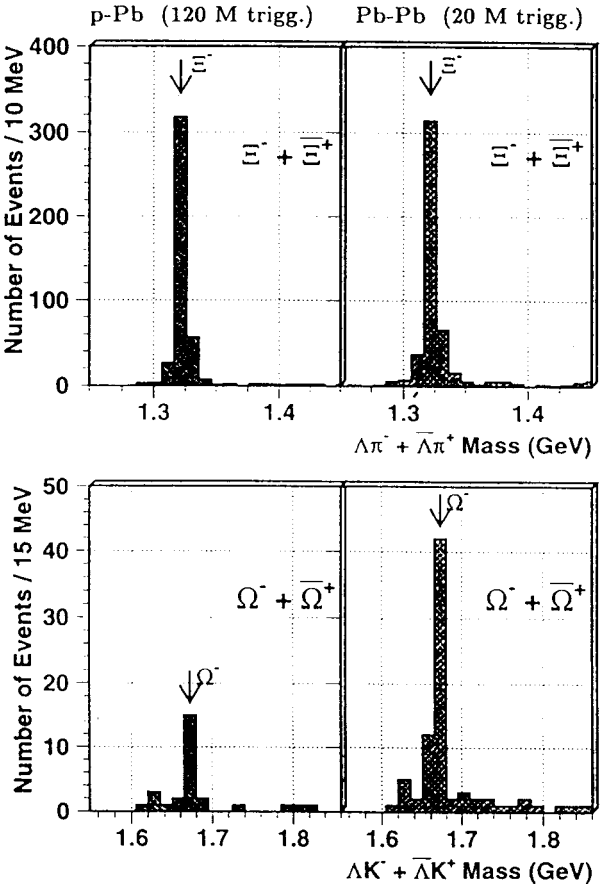

Fig. 24. Ξ and Ω signals in p-Pb and Pb-Pb data

3.4. Bose–Einstein correlations and source size determination in nuclear collisions

The intensity interferometry, or the Hanbury–Brown and Twiss method for the source size determination finds an extensive use in the study of nuclear collisions.

The method consists in analyzing correlations between identical particle pairs. Since there is a separate lecture by Gordon Baym at this School, dedicated to this subject, I will barely cover the basic results without going into details.

Experimentally the two particle correlation function is obtained from the ratio of the two particle probability distribution in relative momentum and the uncorrelated background, usually constructed from particles taken from separate events (identical particles emitted from a chaotic source tend to

group together in momentum space). This ratio is the Fourier transform of a static particle source distribution, determined by its spatial size R. The spatial dimensions of the source can be decomposed into the longitudinal and transverse components.

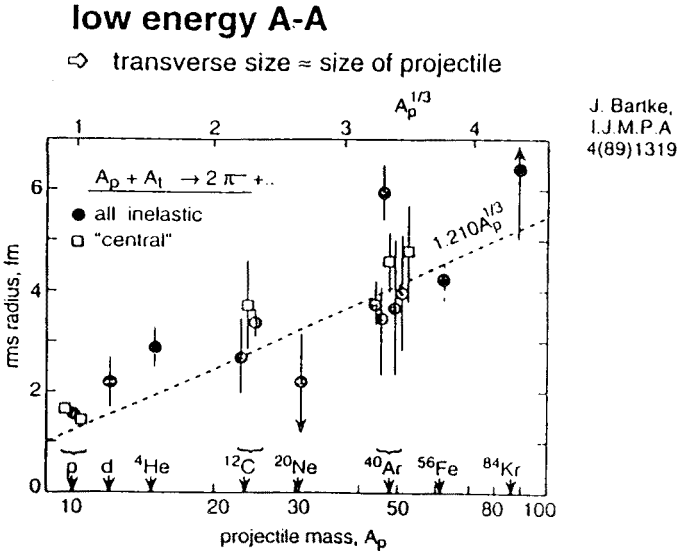

Fig. 25. RMS radius of pion source from low energy (few GeV) nuclear collisions

In nuclear collisions one may reasonably expect that the source is not static but undergoes some space-time evolution. Various authors have demonstrated [28–30] that source evolution translates into a correlation function dependence on both transverse and longitudinal momentum at which the correlation is evaluated.

The results of R determination for pions emitted from low energy nuclear collisions are summarized in Fig. 25 from [31], where the rms values of pion source radius for various combinations of projectiles and targets at the few GeV/N range are shown. The transverse size of the source is roughly proportional to the geometrical radius of the projectile nucleus. Fig. 26 shows the high energy data — the transverse source size plotted as a function of the geometrical radius of interacting matter (to account for various combinations of projectile-target and different centrality cuts) [32]. Again a proportionality is observed — but with the coefficient indicating that the transverse size is larger than just the geometrical radius. Preliminary analysis of the Pb–Pb data indicates a possibility of transversely expanding pion source. In the longitudinal direction, the source dimension, albeit model dependent, presents a simple picture. The rapidity and transverse momentum dependence of R longitudinal is consistent with a longitudinally expanding boost invariant source. This observation holds for oxygen and sulphur

beams incident on nuclear targets, and also for Pb-Pb collisions [33, 34]. A refined multidimensional analysis of two pion correlations offers a wide possibility of interpretation in terms of freeze-out mechanism and particle emission duration.

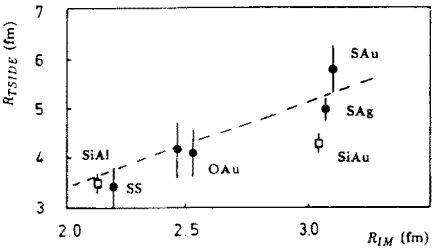

Fig. 26. Transverse source size as a function of rms radius of interacting matter from high energy nuclear collisions.

It is interesting to study the source sizes as determined by different particle species. Here the NA44 experiment offering good particle identification leads the field. Fig. 27 shows their summary of the HBT parameters for pions and kaons as determined for various projectile-target combinations [35]. It is interesting to note that the charged kaons apparently come from a smaller size object than the pions.

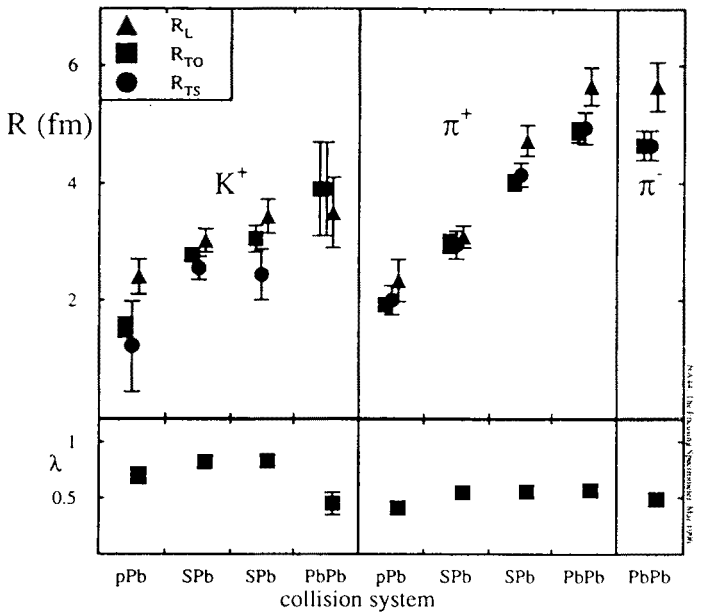

Fig. 27. Summary of HBT parameters from different collisions and for different particles

4. Summary

As stressed at the beginning, this is a very 'down to earth' review with many facts, and little interpretation. Let me just state what are, in my opinion, the most important/promising observations from the 200/158 GeV/N study of nuclear collisions.

1. A clear excess in the mass spectrum of e^+e^- in the range between the mass of two pions and 1.5 GeV/c is observed. Is it thermal pion radiation from a hot source? Does it indicate in-medium effects for vector meson resonances?

2. Large ammount of data on J/ψ and ψ' production are consistent with strong nuclear absorption, parametrized by an effective cross section of about 6 mb. However, a dramatic effect of a J/ψ suppression occurs for central Pb-Pb collisions, not consistent with the above mentioned suppression. Do we see an effect of deconfined matter produced in the hotest region of two heavy nuclei impinged on each other?

3. High energy nuclei are only partially stopped in their collision. The amount of stopping seems to increase for the heaviest objects. A baryon rich region is created around midrapidity for central lead on lead collisions.

4. The transverse mass spectra show a distinct mass dependence and the slope parameters ('temperature') increase with the particle mass. The favorite interpretation seems to be the transverse flow mechanism, where different particles move with the same velocity. An interpretation in terms of a superposition of isotropically decaying fireballs is not excluded.

5. The strangeness enhancement (relative to nucleon-nucleon superposition), observed for sulphur collisions, persists in lead on lead collisions, but does not increase. Cascade hyperon production increase compared to hadron-nucleus collision is clearly observed. A strongest effect is observed for the Ω — albeit with large errors.

6. The interferometric analysis of identical particles reveals a creation of longitudinally expanding source. The transverse size is not in contradiction with some amount of transverse expansion. In collisions of heavy nuclei the kaons seem to be emitted from a smaller region than the pions.

I wish to express my cordial thanks to Profs. Ewa Skrzypczak and Andrzej K. Wroblewski for very helpful comments on this manuscript.

REFERENCES

[1] A. Drees, *Nucl. Phys.* **A610**, 536c (1996).
[2] J. Cleymans *et al.*, *Z. Phys.* **C52**, 517 (1991).
[3] B. Kampfer *et al.*, *Phys. Rev.* **C49**, 1132 (1994).

[4] G.Q. Li *et al.*, *Phys. Rev. Lett.* **75**, 4007 (1995).
[5] G.E. Brown, M. Rho, *Phys. Rev. Lett.* **66**, 2720 (1991).
[6] T. Matsui, H. Satz, *Phys.Lett.* **B178**, 416 (1986).
[7] C. Baglin *et al.*, *Phys. Lett.* **B255**, 459 (1991).
[8] A. Sansoni, *Nucl. Phys.* **A610**, 373c (1996).
[9] E. Braaten, *Nucl. Phys.* **A610**, 386c (1996).
[10] D. Kharzeev, H. Satz, *Phys. Lett.* **B334**, 155 (1994).
[11] G. Herschel, J. Hufner, *Z. Phys.* **C56**, 171 (1992).
[12] M. Gonin *et al.*, *Nucl. Phys.* **A610**, 404c (1996).
[13] C. Lourenco, *Nucl. Phys.* **A610**, 552c (1996).
[14] D. Kharzeev, *Nucl. Phys.* **A610**, 418c (1996).
[15] J. Blaizot, J.Y. Olitraut, *Phys. Rev. Lett.* **77**, 1703 (1996).
[16] P. Jacobs, Contribution to the ICPAQGP97 Conference, Jaipur India, March 1997.
[17] I. Bearden *et al.*, *Phys. Rev. Lett.* **78**, 2080 (1997).
[18] R. Stock, private communication.
[19] A. Leonidov *et al.*, *Nucl. Phys.* **A610**, 124c (1996).
[20] H. Bialkowska *et al.*, *Z. Phys.* **C55**, 491 (1992).
[21] C. Borman, Contribution to the Strangeness in Quark Matter Conference, Santorini, April 1997.
[22] P. Guillaud, *Nucl. Phys.* **A525**, 449c (1991).
[23] V. Friese, Contribution to the Strangeness in Quark Matter Conference, Santorini, April 1997.
[24] T. Matsuda, H. Shiomi, *Nucl. Phys.* **A590**, 545c (1995).
[25] J. Rafelski, *Phys. Lett.* **B262**, 333 (1991).
[26] S. Abatzis *et al.*, *Phys. Lett.* **B393**, 210 (1997).
[27] H. Helstrup, *Nucl. Phys.* **A610**, 165c (1996).
[28] Y.M. Sinyukov, *Nucl. Phys.* **A498**, 151c (1989).
[29] G. Bertsch, *Nucl. Phys.* **A498**, 173c (1989).
[30] U. Heinz *et al.*, *Phys. Lett.* **B382**, 181 (1996).
[31] J. Bartke, *Int. J. Mod. Phys.* **A4**, 1319 (1989).
[32] P. Seyboth, *Nucl. Phys.* **A544**, 293c (1992).
[33] K. Kadija, *Nucl. Phys.* **A610**, 248c (1996).
[34] T. Alber *et al.*, *Z. Phys.* **C66**, 77 (1995).
[35] A. Franz, *Nucl. Phys.* **A610**, 240c (1996).
[36] T. Alber *et al.*, *Phys. Rev. Lett.* **75**, 3814 (1995).